



Upper mantle anisotropy beneath Peru from SKS splitting: Constraints on flat slab dynamics and interaction with the Nazca Ridge

Caroline M. Eakin^{a,*}, Maureen D. Long^a, Lara S. Wagner^b, Susan L. Beck^c, Hernando Tavera^d

^a Department of Geology and Geophysics, Yale University, New Haven, CT, USA

^b Department of Geological Sciences, University of North Carolina at Chapel Hill, Chapel Hill, NC, USA

^c Department of Geosciences, University of Arizona, Tucson, AZ, USA

^d Instituto Geofísico del Perú, Lima, Peru

ARTICLE INFO

Article history:

Received 11 September 2014

Received in revised form 5 December 2014

Accepted 7 December 2014

Available online xxxx

Editor: P. Shearer

Keywords:

seismic anisotropy

shear wave splitting

flat slab subduction

Nazca Ridge

South America

ABSTRACT

The Peruvian flat slab is by far the largest region of flat subduction in the world today, but aspects of its structure and dynamics remain poorly understood. In particular, questions remain over whether the relatively narrow Nazca Ridge subducting beneath southern Peru provides dynamic support for the flat slab or it is just a passive feature. We investigate the dynamics and interaction of the Nazca Ridge and the flat slab system by studying upper mantle seismic anisotropy across southern Peru. We analyze shear wave splitting of SKS, sSKS, and PKS phases at 49 stations distributed across the area, primarily from the PerU Lithosphere and Slab Experiment (PULSE). We observe distinct spatial variations in anisotropic structure along strike, most notably a sharp transition from coherent splitting in the north to pervasive null (non-split) arrivals in the south, with the transition coinciding with the northern limit of the Nazca Ridge. For both anisotropic domains there is evidence for complex and multi-layered anisotropy. To the north of the ridge our *KS splitting measurements likely reflect trench-normal mantle flow beneath the flat slab. This signal is then modified by shallower anisotropic layers, most likely in the supra-slab mantle, but also potentially from within the slab. To the south the sub-slab mantle is similarly anisotropic, with a trench-oblique fast direction, but widespread nulls appear to reflect dramatic heterogeneity in anisotropic structure above the flat slab. Overall the regional anisotropic structure, and thus the pattern of deformation, appears to be closely tied to the location of the Nazca Ridge, which further suggests that the ridge plays a key role in the mantle dynamics of the Peruvian flat slab system.

© 2014 Elsevier B.V. All rights reserved.

1. Introduction

Episodes of flat or shallow subduction are often associated with volcanic gaps, increased intra-plate seismic energy release, and widespread deformation of continental interiors (e.g. Gutscher, 2002). Despite the significant impact of flat subduction upon the surface, and the prominence of shallow subduction worldwide today (representing ~10% of subduction zones globally; Gutscher et al., 2000), the formation, evolution and dynamics of flat slabs remain poorly understood. For example, there has long been a suggestion that flat slabs result from the subduction of thick oceanic crust, such as plateaus, but the global correlation between such oceanic features and shallow subduction is imperfect (Skinner and Clayton, 2013).

Even at the regional scale, for the Peruvian flat slab, open questions exist over the importance of the Nazca Ridge, which is presently subducting beneath southern Peru, considering the large difference in size between the Nazca Ridge (~200 km wide) and the flat slab segment (~1500 km wide). Investigation of the mantle flow field surrounding the Peruvian flat slab, particularly in the vicinity of the Nazca Ridge, has the potential to shed light on the dynamics and inner workings of this and other flat slab systems. Our goal is therefore to explore the interaction between the ridge and the flat slab from the point of view of how the surrounding mantle deforms. In this way we hope to better understand what role, if any, the Nazca Ridge plays in the development of the flat slab.

Over the last few decades shear wave splitting has become an invaluable tool for probing seismic anisotropy and the dynamics of the earth's interior. Seismic anisotropy describes the directional dependence of seismic wave speed. Shear wave splitting is the process whereby a shear wave passing through such an anisotropic

* Corresponding author.

E-mail address: caroline.eakin@yale.edu (C.M. Eakin).

medium is polarized into two quasi-S waves with distinct polarizations in a fast direction (ϕ) and a slow direction. The two waves travel at different velocities through the medium and therefore accumulate a delay time (δt) between their arrivals on the seismogram. The size of the delay time accrued depends on the strength of the anisotropy and the length of the path through the anisotropic material (which is proportional to the thickness of the anisotropic layer).

One of the most significant anisotropic domains within the earth is in the upper mantle, in which strain (deformation) in the dislocation creep regime results in the lattice preferred orientation (LPO) of anisotropic minerals such as olivine (e.g. Karato et al., 2008). This non-random distribution of crystallographic axes results in an effective bulk anisotropy that is detectable by seismic waves. Armed with knowledge of the relationship between mantle strain and LPO fabric geometry, we can exploit observations of seismic anisotropy to infer the orientation of deformation and flow in the upper mantle.

For olivine, the most abundant upper mantle mineral, there are several known LPO fabrics (most commonly A-, B-, C-, D-, and E-types) that occur under different physical and chemical conditions, such as temperature, stress, and water content (Jung and Karato, 2001; Jung et al., 2006; Karato et al., 2008; Katayama et al., 2004). Each fabric type represents different 3D orientations of the crystallographic axes with respect to a given strain geometry. Under conditions typical of the upper mantle, A-, C-, or E-type fabrics are most likely, and for all three fabrics the fast splitting direction tends to align with the direction of shear (Karato et al., 2008). Under low temperature, high stress and water rich conditions, as expected in the fore-arc mantle wedge (Kneller et al., 2007, 2005), B-type fabric likely dominates. In this regime, the fast axis aligns within the shear plane, orthogonal to the shear direction (Jung and Karato, 2001; Jung et al., 2006).

Shear wave phases that pass through the core, such as SKS, are particularly well suited for probing upper mantle anisotropy. These phases are polarized in the radial direction upon conversion from a P wave in the liquid outer core, thus removing any effect from seismic anisotropy on the source side. They are sensitive to anisotropy anywhere along their paths from the core–mantle boundary to the receiver. In most cases, however, contributions from D'' , the lower mantle, and the crust are thought to be minimal, with upper mantle anisotropy making the dominant contribution to the signal. This is evidenced by, for example, a first order global correlation between SKS splitting observations and predictions based on surface plate motions and geodynamic models of mantle flow (e.g. Conrad et al., 2007; Long and Becker, 2010; Walpole et al., 2014).

Occasionally SKS phases arrive at seismic stations displaying no signs of having been split, in what is known as a null measurement. This can occur when the initial SKS polarization is aligned with the fast or slow axis of anisotropy; therefore, null measurements can be useful in constraining the anisotropic orientation. When stations are dominated by null measurements over a wide range of backazimuths, however, this can signify an isotropic (or weakly anisotropic) upper mantle, destructive interference of two or more layers of anisotropy, or a vertical axis of (transversely isotropic) symmetry. The last option is typically interpreted as vertical mantle flow, either in the form of active mantle upwelling, e.g., beneath Bermuda (Benoit et al., 2013), or down-welling, e.g., for a proposed lithospheric drip beneath Nevada (West et al., 2009).

Simple correlations between SKS splitting (or nulls) and flow in the upper mantle break down, however, around subduction zones (e.g. Long and Silver, 2008, 2009), where mantle flow is likely more complex and the interpretation of SKS splitting becomes increasingly difficult. A factor in this difficulty is the possibility of

multiple domains of anisotropy, with potential contributions from the sub-slab mantle, slab, mantle wedge, and overriding plate. Additional complications may also arise from the effects of slab dip and volatile influx. In particular, the presence of water can significantly affect the olivine LPO fabric geometry and the distribution of highly anisotropic hydrous phases such as serpentine. Challenges in interpreting SKS splitting measurements in subduction systems are confounded when using data from temporary seismic arrays, which are usually deployed for ~ 2 yr. In this case, it is often difficult to acquire sufficient backazimuthal coverage to discriminate among single-layered, multi-layered and/or dipping anisotropy (e.g. Eakin et al., 2010).

In this study we use data from the temporary PULSE (PerU Lithosphere and Slab Experiment) deployment located over the Peruvian flat subduction zone (Fig. 1). This location provides several advantages that ameliorate some of the challenges inherent in interpreting SKS splitting in a subduction zone. First, in the flat subduction regime, once the slab approaches ~ 100 km depth the slab dip angle is very shallow ($\sim 10^\circ$) (Cahill and Isacks, 1992; Hayes et al., 2012), so dipping anisotropy is less likely. Second, there is no substantial mantle wedge to consider; at most only a thin layer of mantle (~ 30 km) remains between the flat slab and overlying continental crust, and directly above the Nazca Ridge this layer is absent (Bishop et al., 2013; Phillips and Clayton, 2014). Third, previously published studies of local direct S and source-side teleseismic S phases independently constrain the supra-slab and sub-slab anisotropy, respectively (Eakin and Long, 2013; Eakin et al., 2014). Fourth, a detailed analysis of SKS splitting at the long-running GSN station NNA, located in our study area, has provided sufficient sampling in backazimuth and frequency to constrain multiple layers of anisotropy (Eakin and Long, 2013). This permanent station therefore provides us with a valuable benchmark with which to compare and contrast SKS splitting measured at our temporary stations.

SKS splitting provides a depth-integrated view of upper mantle anisotropy, and is therefore particularly useful for looking at lateral variations in anisotropic structure. Complementary to this, splitting from local and source-side S phases provide important information about anisotropy within different sub-domains of the subduction zone (i.e. sub-slab vs. wedge anisotropy), but their interpretation can be hampered by the heterogeneous and often biased distribution of slab seismicity. In contrast, the nearly vertical propagation of SKS phases ensures efficient sampling of the upper mantle beneath seismic stations and thus provides a more uniform sampling of regional anisotropic patterns. SKS splitting thus provides an ideal tool for exploring lateral variations in upper mantle anisotropy beneath southern Peru and understanding how those variations relate spatially to Nazca Ridge subduction, thus shedding light on the dynamic interactions between the ridge and the flat slab. In this study we document a sharp contrast in anisotropic structure, and therefore mantle deformation, in association with the Nazca Ridge. This is illuminated by the SKS splitting patterns, which show apparent splitting north of the ridge (mostly likely reflecting a combination of multiple layers of anisotropy), while nulls are pervasive directly over the ridge and to its south.

2. Peruvian flat slab subduction and the Nazca Ridge

The Peruvian flat slab subduction zone extends 1500 km along strike from 3°S to 15°S , representing the largest region of flat subduction in the world today (Cahill and Isacks, 1992; Hayes et al., 2012). Based on seismicity patterns (Cahill and Isacks, 1992), receiver functions (Phillips and Clayton, 2014), and surface wave tomography (Ma and Clayton, 2014), the slab appears to flatten at around 100 km depth, and continues for several hundred kilometers inboard before steepening and re-subducting into the mantle.

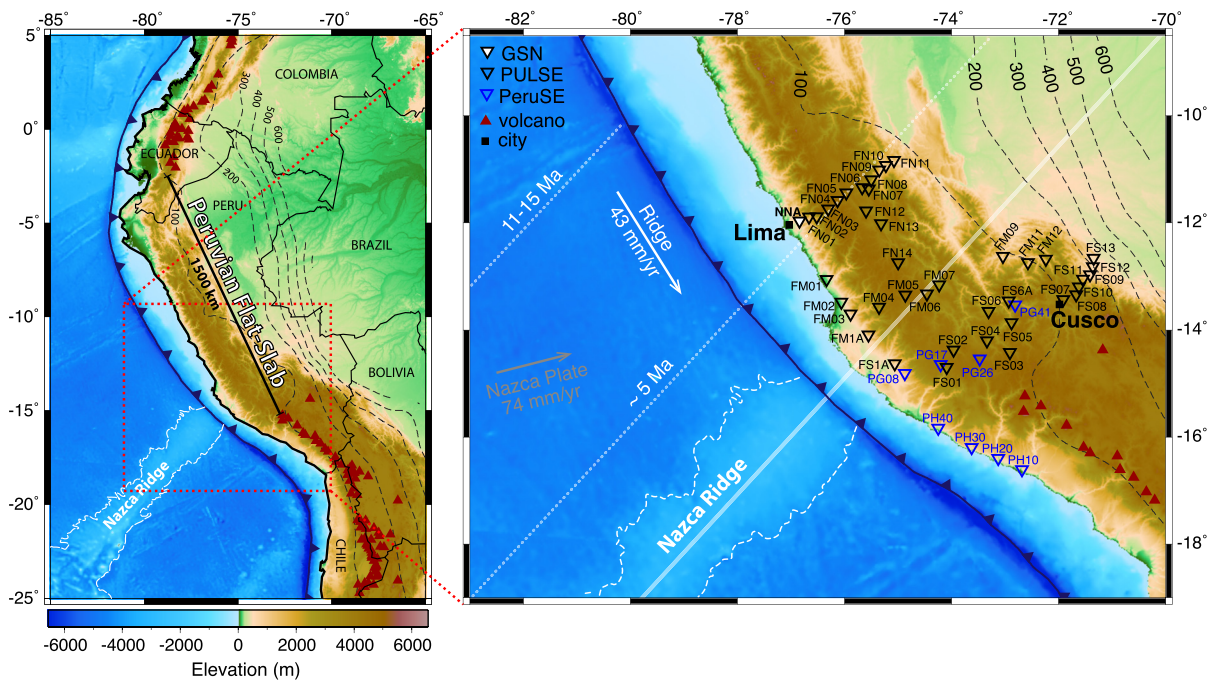


Fig. 1. Tectonic setting and station locations. Slab contours (dashed dark gray lines) are from the Slab 1.0 model (unit: km) (Hayes et al., 2012). Map on the right shows distribution of stations (inverted triangles color coded by seismic network) used in this study, with station names shown. Thick white line shows continuation of the subducted Nazca Ridge. Dotted white lines show estimated position of the ridge in the past (Hampel, 2002). Grey arrow represents the absolute plate motion of the Nazca plate in a hotspot reference frame from HS3-NUVEL1A (Gripp and Gordon, 2002). Volcano locations (red triangles) are from Siebert and Simkin (2002). (For interpretation of the references to color in this figure legend, the reader is referred to the web version of this article.)

At the surface the flat slab is most easily recognized by the stark paucity of contemporary arc volcanism (Fig. 1), in contrast to the more steeply dipping ($\sim 30^\circ$) subduction regimes to the north and south. The lack of volcanism above the flat slab is most likely due to the constriction of the mantle wedge and therefore restricted asthenospheric corner flow (e.g. Barazangi and Isacks, 1976). Only a thin mantle layer ($\sim 30\text{--}50$ km thick) exists between the slab and the overlying continental crust, which is approximately 50–70 km thick (Assumpção et al., 2013; Feng et al., 2007; Lloyd et al., 2010; Van der Meijde et al., 2013; Phillips and Clayton, 2014).

Another distinctive characteristic of the region that spatially coincides with the flat slab is the subduction of the Nazca Ridge at $14\text{--}17^\circ\text{S}$ on the Peru–Chile Trench (Fig. 1). The Nazca Ridge is a linear aseismic ridge feature on the Nazca plate that lies offshore of southern Peru. It is thought to have formed at the Pacific–Farallon (now Pacific–Nazca) spreading center during the Cretaceous and is associated with the Easter hotspot (Hampel et al., 2004; Pilger, 1981; Pilger and Handschumacher, 1981; Woods and Okal, 1994). The Nazca Ridge first intersected the Peru–Chile trench around $9\text{--}11^\circ\text{S}$ approximately 11–15 million years ago, and subsequently migrated southward at a relative velocity of 43 mm/yr due to the oblique plate convergence (Hampel, 2002; Rosenbaum et al., 2005) (Fig. 1).

Offshore, the Nazca Ridge is over 1000 km long and 200 km wide and sits at an elevation of 1500 m above the surrounding seafloor (Hampel, 2002). Seismic and gravity surveys indicate that the ridge has an unusually thick crust ($\sim 17\text{--}18$ km), of which two thirds is gabbroitic lower crust (Couch and Whitsett, 1981; Hampel et al., 2004; Woods and Okal, 1994). The positive buoyancy of this subducting thickened oceanic crust is evidenced by enhanced tectonic erosion at the margin, the westward shift of the coastline, and the uplift of the Fitzcarrald Arch, a 500 km wide topographic high (mean elevation ~ 600 m) in the Amazonian foreland (Espurt et al., 2007; Hampel et al., 2004).

A global correlation between areas of flat or shallow subduction and over-thickened oceanic crust in the subducting plate has long

been noted (e.g. Gutscher et al., 2000), but the strength and universality of this correlation has recently been questioned (Skinner and Clayton, 2011, 2013). In the case of Peru, it is clear that the subducting Nazca Ridge is relatively buoyant, it is unclear however whether this feature provides dynamic support to the whole length of the Peruvian flat slab. The Nazca Ridge has been sweeping south through Peru over the past ~ 15 Ma, suggesting a possible correlation between the presence of the ridge and slab flattening. At present, however, the Nazca slab is flat over a wide area, spanning ~ 1500 km along strike (see black bar in Fig. 1). This includes the northern end of the flat slab region (north of 9°S), which has never experienced the subduction of the Nazca Ridge. It has been suggested that the northern portion of the flat slab experienced subduction of a different buoyant feature known as the Inca Plateau (Gutscher et al., 1999), but this is disputed (Skinner and Clayton, 2013). Major questions therefore remain over how the Nazca Ridge interacts with the Peruvian flat slab and what role the ridge plays in the dynamics of the flat subduction system. The goal of this study is therefore to understand the present-day dynamics and deformational history of the region, by analyzing how seismic anisotropy varies both laterally and with depth across the subduction zone.

3. Data and methods

We investigate shear wave splitting at 49 broadband seismic stations located throughout the flat slab region of southern Peru (Fig. 1). The majority of these stations (40 out of 49) belong to the recent PULSE (PerU Lithosphere and Slab Experiment) deployment, which was in operation from October 2010 until June 2013. We also used data from 8 stations belonging to PeruSE (Peru Subduction Experiment), which operated concurrently from November 2010 until April 2013. Finally, we reinvestigate data from permanent station NNA over the same time period. This station is located near Lima, and belongs to the Global Seismographic Network (GSN). It is the only long-running station located

in the region, and provides an extended record (>20 yr) of shear wave splitting (Helffrich et al., 1994; Kaneshima and Silver, 1995; Eakin and Long, 2013).

We analyze all teleseismic events of magnitude 6.0 and greater for the presence of splitting of various shear wave phases. Specifically, we study SKS and sSKS phases in the epicentral distance range 88°–130°, and PKS phases in the range 130°–150°, in an attempt to increase backazimuthal coverage. SKKS phases did not prove to be useful, due to a lack of suitable events at backazimuths different than those already well sampled by SKS and PKS, and so were omitted from our study. At such distances the arrivals have almost vertical incidence (<10° for SKS, and <13° for PKS).

The shear wave splitting analysis was performed with the SplitLab software package (Wüstefeld et al., 2008). Two independent splitting measurement methods were applied to estimate the splitting parameters (fast direction: φ , and delay time: δt): the transverse component minimum energy (SC) method of Silver and Chan (1991), and rotation-correlation (RC) method (Bowman and Ando, 1987). We only retained measurements which yielded consistent estimates with both measurement methods; henceforth we present results obtained via the SC method as it is stable over the widest range of backazimuths (Wüstefeld and Bokelmann, 2007). In all cases a bandpass filter was applied, with variable cutoff frequencies, in order to best enhance the signal-to-noise ratio on each individual seismogram. The low frequency cutoff varied from 0.02–0.06 Hz, and the high frequency cutoff from 0.09–0.35 Hz. Even though variable bandpass filters have been applied, in general the *KS phases typically contain energy at ~0.08 Hz (characteristic period of ~12.5 s; see Fig. S1 of the supplementary material). We therefore do not expect our results to be strongly influenced by frequency-dependent effects. This is further demonstrated by Fig. S2.

All the splitting measurements were visually inspected and underwent quality control, with both qualitative and quantitative conditions applied. Quantitative conditions included a signal-to-noise ratio (SNR) cutoff greater than 5, and errors less than 1 s in δt and less than 22.5° in φ at the 95% confidence level. Additionally, we required agreement between the RC and SC methods with $|\Delta\varphi| < 22.5^\circ$, and $\delta t_{\text{RC}}/\delta t_{\text{SC}} > 0.7$ (Wüstefeld and Bokelmann, 2007). Qualitative measures included the observation of similarly shaped shear wave pulses on the estimated fast and slow directions, minimal energy on the corrected transverse component, and linearization of the original elliptical particle motion following the correction for splitting. An example of a well-constrained splitting measurement is shown in Fig. S3.

Observations of null *KS arrivals were also recorded in this study. In this case we required a clearly visible shear phase on the radial component with little energy on the uncorrected transverse component (i.e. linear uncorrected particle motion). Again, we applied an SNR cutoff greater than 5. For an example of a null measurement see Fig. S3. In general, null arrivals suggest that the shear wave has not undergone any splitting. There can be various explanations for this; for example, the upper mantle beneath the receiver is isotropic, or has strongly heterogeneous anisotropy (and thus effective isotropy), or the incoming polarization of the phase (i.e. backazimuth for *KS phases) is aligned with the fast or slow axis of anisotropy.

4. Shear wave splitting results

Our analysis yielded 234 splitting measurements and 341 null observations from teleseismic *KS phases arriving at the 49 stations across southern Peru (Fig. 2a). We observed distinct differences in the spatial distribution of split and null results across the region. A first-order pattern of robust splitting measurements predominates in the northern section of the array, while nulls

dominate towards the south (Fig. 2b). The transition from robust splitting to predominantly nulls appears to occur at a latitude of ~13°S, and is exemplified by the record section displayed in Fig. 3. In this example, a clear SKS arrival is observed on the transverse component across the northern (FN) stations in all frequency bands, but towards the south (stations beginning with FM and FS) it becomes increasingly difficult to pick out the SKS energy on the transverse component above the background noise, indicating that the shear phase has not been split upon arrival at the station.

Focusing on the northern group of stations (labeled FN in Fig. 1), we observe consistent splitting with fast directions oriented approximately NW–SE (blue–purple–magenta bars in Fig. 2a), roughly trench-parallel. In this sub-dataset, 69% of the measurements are splits (157 splits, 71 nulls), and the mean splitting parameters are -62° for φ , and 1.23 s for δt . As is typical for the region, the backazimuthal distribution of these results is relatively limited (Fig. 4), so backazimuthal variations in apparent splitting cannot be ruled out. The vast majority of events in our study (74%) originate from the Tonga subduction zone, and therefore arrive from southwesterly backazimuths. The backazimuths of most of the remainder differ mostly by ~90°, arriving from the northwest. With that caveat, however some backazimuth variability is present at a few of the northern stations; in particular, we observe an apparent rotation in φ over the backazimuth range 45°–75° at stations NNA, FN01, FN05, FN13, FM01 (Fig. S4) as well as variability in δt over the same range. This is consistent with previous measurements by Eakin and Long (2013) at station NNA over a longer 20 yr time period, which revealed a robust rotation in φ over the same backazimuth range and over different frequency bands. This trend was used to constrain models of multiple layers of anisotropy beneath NNA. The 10 best-fitting two-layer models that were found to match the observations in the Eakin and Long (2013) study are plotted in Fig. S4. Although our results are often clustered within a narrow backazimuthal range, and therefore cannot resolve the number of anisotropic layers present, our new measurements are not inconsistent with the best fitting two-layer models from Eakin and Long (2013).

For the southern group of stations, null observations become much more predominant, representing 81% of the measurements (198 nulls compared to 47 splits). These dominantly null stations cover a large area of southern Peru (Fig. 2b), and there are indications that this characteristic pattern continues to the south of our array (Biryol et al., 2013). As was the case further to the north, the backazimuthal distribution of these null results is limited (Fig. 4), although nulls do persist over the backazimuth range that is well-sampled (~40°–75°). We further note that null arrivals are often observed from events arriving from 2 or 3 different backazimuth quadrants (see, for example, FM02–07, FM09, FM12, FS03, FS05, FS06, FS1A, FS6A, PG08, PG26, PH10, PH20 stereoplots in Fig. S5). We often observe a small number of split measurements at these null-dominated stations (~1–2 per station), but their orientations are scattered and geographically variable. Often their delay times are also either modest (45% less than 1 s) or quite large (28% more than 1.5 s), which can often be an indication that the measurement is actually approaching a ‘near-null’ (Wüstefeld and Bokelmann, 2007) and is poorly constrained.

A third group of 7 stations located in a line to the east of Cusco displays a different set of characteristics (Fig. 2 and Fig. S5). At these stations there are still many nulls (72 measurements out of 102) recorded over the same available range of backazimuths, but there are also a substantial number of splits (30 measurements, or 29% of the sub-dataset). The fast directions of these splits tend to align west to northwest (mean φ : -65° ; blue/purple bars in Fig. 2a), similar to the orientations found for the northern stations. The delay times, however, tend to be larger (mean δt is 1.7 s), and

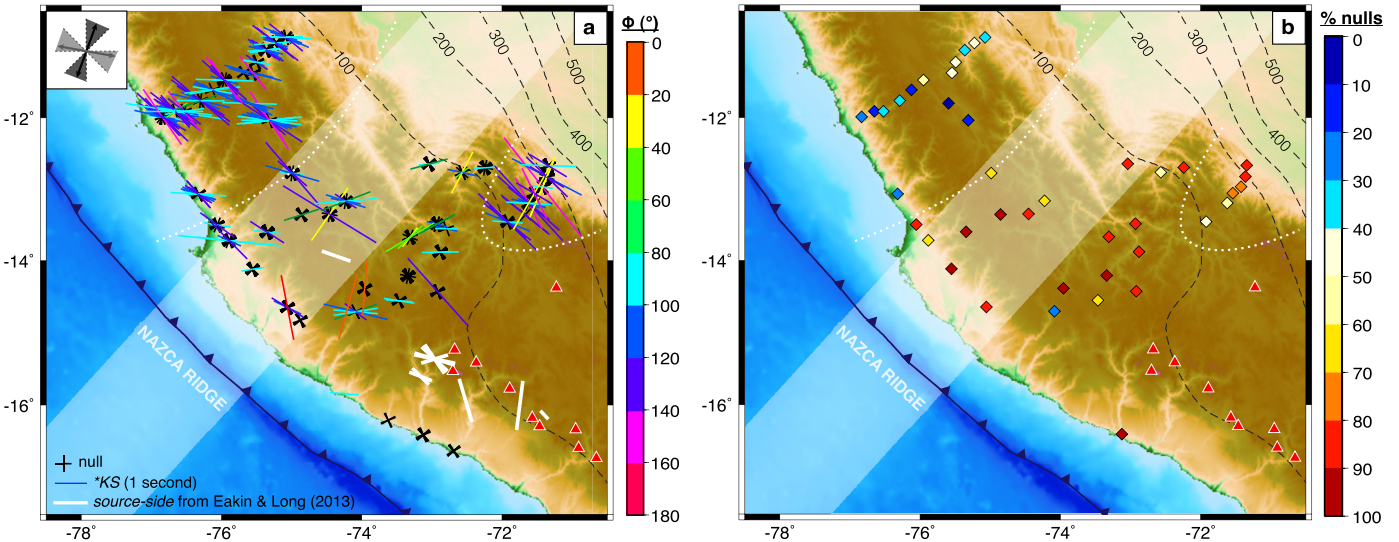


Fig. 2. (a) Map of individual SKS, sSKS, and PKS shear wave splitting measurements made at each station. Each *KS splitting measurement is represented by a bar, oriented and colored by ϕ (see color scale on the right). The length of the bar is scaled by δt (1 s example shown in the legend in bottom left corner). Null measurements are represented by small black crosses aligned according to the possible fast/slow directions, based on the backazimuth of the event. The region has three distinct zones of shear wave splitting patterns, which are delineated by the dotted white lines. Thick white bars are source-side splitting measurements from Eakin and Long (2013) that represent anisotropy of the mantle beneath the slab, plotted at the event location. The two-layer anisotropic model found at station NNA by Eakin and Long (2013) is shown in the box in the upper left corner. The lower layer is represented by dark gray and the upper layer by pale gray. The gray thick arrows represent the best model, while the shaded regions represent the acceptable range of best-fitting models. Transparent white band across the region highlights the estimated position of the subducting Nazca Ridge. Dashed slab contours and volcano locations are the same as for Fig. 1. (b) Map of the percentage of nulls relative to the total number of measurements (splits and nulls) at each station. Stations with less than five measurements in total are not included on the map. Stations north of the Nazca Ridge are dominated by split results (blue diamonds) whilst towards the south they are dominated by null results (red diamonds). (For interpretation of the references to color in this figure legend, the reader is referred to the web version of this article.)

it does not appear that the splitting parameters vary significantly with backazimuth (Fig. S5).

5. Discussion

It is clear from the results described above that the anisotropic structure of the Peruvian flat slab region varies significantly along strike, with split *KS arrivals dominating in the north and nulls dominating to the south. An important step in the interpretation of this dataset is to understand the origin and implications of the geographic variability in measured splitting patterns.

For the northern stations, it is clear that the measured NW–SE oriented fast splitting directions appear consistently trench-parallel. This orientation agrees with early studies of shear wave splitting at stations NNA (near Lima) and CUS (near Cusco) in the region (Helffrich et al., 1994; Kaneshima and Silver, 1995), and also with the classic interpretation by Russo and Silver (1994) of trench-parallel sub-slab mantle flow along the South American margin induced by trench rollback (Fig. 6). Both these early studies and the results presented here are, however, based on only a few years worth of data, and are severely hindered by the limited backazimuthal coverage. This limitation is particularly acute for South America, which generally suffers from poor backazimuthal coverage at the epicentral distances relevant for core phases. With measurements over a limited backazimuthal range it is difficult to rule out complex anisotropy, which would complicate the interpretation of fast splitting directions.

Our previous work at station NNA, using the full 20+ years of data recording, produced evidence for frequency dependent and backazimuthally variable splitting parameters, indicating the presence of complex, multi-layered anisotropy (Eakin and Long, 2013). When we revisit NNA to measure shear wave splitting over a more limited time frame such as the PULSE deployment (~ 2.5 yr), we find that it is not possible to detect the same level of detail or variability in the results that would be diagnostic of anisotropy

beyond a single flat homogeneous layer. This is demonstrated in Fig. 5, which shows that the misfit for the best one-layer model of anisotropy is similar to that for the best two-layer model of anisotropy; therefore, it is not possible to distinguish between single versus multiple layers of anisotropy using the PULSE dataset alone.

Given the similarity in fit between the one- and two-layer models, we would normally opt for the simplest model to explain our results: i.e. a single layer of anisotropy with fast axes orientated trench-parallel (mean $\phi \sim 62^\circ$), and such a model is entirely valid. There is, however, prior information available from Eakin and Long (2013), who showed that it is possible constrain two layers of anisotropy at permanent station NNA when the full 20+ years of data recorded there were used. Interestingly, when we confine ourselves to the time period of the PULSE deployment, the shear wave splitting pattern found across the northern PULSE stations is very similar to that resolved at NNA with the same 2.5 yr of data (Fig. 2a and Fig. S5). We note, additionally, that the misfit level between the splitting results at the northern PULSE stations and predictions of the best two-layer model from Eakin and Long (2013) is comparable to the model misfit at NNA over the same time period (red line, Fig. 5).

Based on these observations and the proximity of the PULSE northern line to permanent station NNA, we therefore suggest that beneath the central part of the Peruvian flat slab (i.e. beneath the northern PULSE stations) there are probably at least two layers of anisotropy present. The range of best fitting models found by Eakin and Long (2013) at NNA suggests that the lower layer is most likely oriented N–S to NE–SW (approaching trench-normal), while the upper layer is oriented E–W to NW–SE (approaching trench-parallel) (see upper left corner of Fig. 2a). If the lower layer corresponds to strain in the sub-slab mantle, then the likely range of fast directions (0° – 45°) is compatible with source-side shear wave splitting measurements from the flat-slab region (Eakin and Long, 2013). These source-side measurements directly isolate the

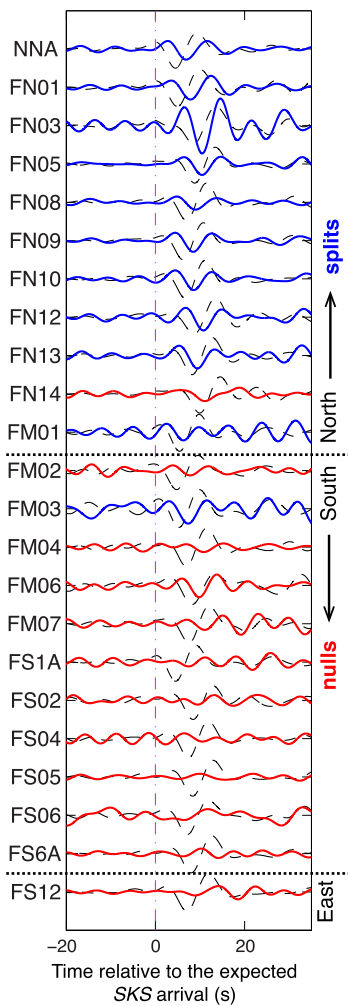


Fig. 3. Record section of a single event ($M_w = 6.4$ originating in the Tonga subduction zone on 11th May 2013 at 20:46:57) arriving from the southwest, highlighting the transition from splitting of SKS phases in the north to nulls in the south. The transverse component is plotted in color, and the radial component in dashed black. The transverse component is colored blue if a well-constrained splitting measurement was made at that station, versus red if it was a null. Significant SKS energy on the transverse component indicates splitting. All traces are scaled such that the radial component is normalized to amplitude 1; the transverse component amplitudes were multiplied by 2 after normalization to aid visibility of the SKS phase (or lack thereof). Station names are listed on the left (see Fig. 1 for their locations). Dotted black horizontal lines represent the same spatial boundaries as the dotted white lines in Fig. 2. All seismograms were bandpass filtered from 0.04 to 0.15 Hz. (For interpretation of the references to color in this figure legend, the reader is referred to the web version of this article.)

anisotropic contribution from the sub-slab mantle and while there is scatter in the results, most of the fast directions are approximately trench-normal (Fig. 7). It therefore seems likely that the mantle flow direction beneath the flat-slab in central Peru is actually closer to trench-normal (assuming A-, C- or E-type olivine LPO fabric), an interpretation that at first glance contrasts with the simplest understanding of generally trench-parallel $*KS$ fast directions observed at the surface.

In comparison, local S splitting measurements (that sample supra-slab anisotropy) over the same region (Eakin et al., 2014) show predominantly trench parallel fast directions (Fig. 7). These are similar to the $*KS$ splitting pattern and in rough agreement with the upper layer of the range of best fitting two layer models from Eakin and Long (2013), although the upper layer may trend slightly more east-west (see Fig. 2a). The local S delay times are, however, much smaller on average (mean $\delta t = 0.27$ s) compared to the $*KS$ (mean $\delta t = 1.24$ s) and the modeled up-

per layer ($\sim 1\text{--}2.5$ s). This discrepancy may be due in part to the differing frequency content (local $S \sim 1.2$ Hz versus teleseismic $*KS \sim 0.08$ Hz). We have previously argued that the local S splitting mainly reflects anisotropy in the thin mantle layer between the flat slab and the continental crust and proposed that the migration of the Nazca Ridge across the southern flat-slab region produced shearing of the mantle, generating olivine fabric with a trench parallel fast direction (Eakin et al., 2014).

Based on the local S and source-side results we therefore have additional evidence that is independent of our $*KS$ dataset for at least two layers of anisotropy in this region: trench-normal anisotropy in the mantle beneath the slab and trench-parallel anisotropy in the mantle above the slab. The discrepancy in delay time between the supra-slab local S results and the modeled upper layer hints that an additional third layer of anisotropy may be required to fully explain the data, perhaps located within the slab. Eakin and Long (2013) did, however, test for the possibilities of three layers of anisotropy beneath NNA; we found that a third layer, while possible, could not be constrained by the available data, unlike the two-layer structure described previously. If the slab were anisotropic, however, then the most likely source would be from anisotropy frozen in at the paleo-spreading center. Based on the present-day orientation of the East Pacific Rise and plate motion direction, we would expect trench-oblique φ (\sim ENE) within the subducting Nazca slab. When combined with a layer of trench-parallel φ above the slab, as seen by the local S splitting, then this could produce constructive or destructive interference (i.e. both larger or smaller delay times) depending on the initial polarization direction.

Moving further south along strike, the NW-SE fast direction pattern of the northern stations transitions into mostly null observations for the middle (FM) and southern (FS) PULSE stations. The geographical location of this transition appears to correlate with the northern boundary of the subducting Nazca Ridge (Fig. 2). This is also co-located with a transition in local S splitting patterns (Eakin et al., 2014) from trench parallel north of the ridge, to null measurements directly over the ridge (Fig. 7). Unlike the local S results, however, which transition back to relatively strong but variable splitting south of the ridge, the $*KS$ results continue to be dominated by nulls throughout the southernmost extent of our study area. This is the first indication of pervasive null $*KS$ arrivals in the area, and was largely unexpected. Other teleseismic shear wave splitting studies over the central Andes in the region of the orocline (below 17°S) show relatively strong coherent splitting (e.g. Polet et al., 2000; Bock et al., 1998; Wölbbern et al., 2014), suggesting that the dominantly null region must end somewhere to the south of our study region (Fig. 6). So while the northern extent of the nulls appears bounded by the northern limit of the subducting ridge, its southern extent is currently unknown but stretches at least as far as the end of the flat slab region. The origin of this predominantly null splitting pattern is therefore rather curious.

There are many potential explanations for the observation of null $*KS$ arrivals. First, the initial polarization direction of the wave (corresponding to the backazimuth for core phases) may be aligned in the fast or slow direction of the anisotropic medium. Second, vertical mantle flow may dominate beneath the station; if there are lateral gradients in flow velocity, a vertical fast symmetry axis would result, leading to little or no splitting of $*KS$ phases. A third possibility is that the upper mantle is isotropic. Fourth, there may be two layers of anisotropy with orthogonal fast directions, leading to destructive interference. A fifth possibility is that the upper mantle is anisotropic, but there is strong heterogeneity present, leading to an effectively isotropic medium on the length scale relevant for $*KS$ waves.

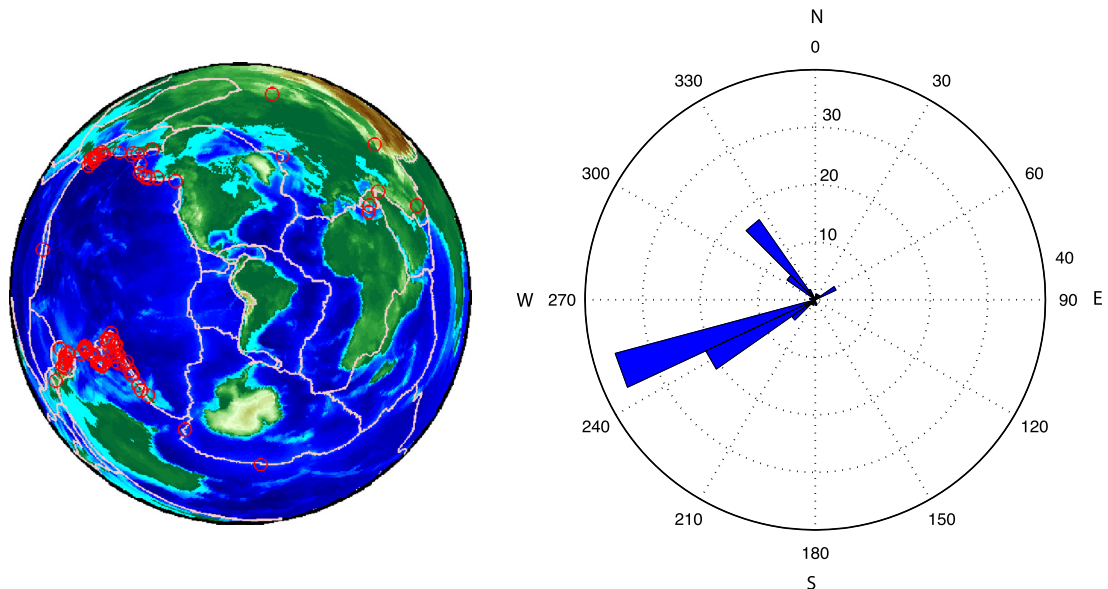


Fig. 4. Distribution of all the events which yielded shear wave splitting results. On the left is a world map of the events (red circles). On the right is a rose histogram of the event backazimuth distribution (10° bins). The majority of events come from the Tonga subduction zone; the Aleutians also provide some suitable events, but these are generally separated in backazimuth by $\sim 90^\circ$ from Tonga. (For interpretation of the references to color in this figure legend, the reader is referred to the web version of this article.)

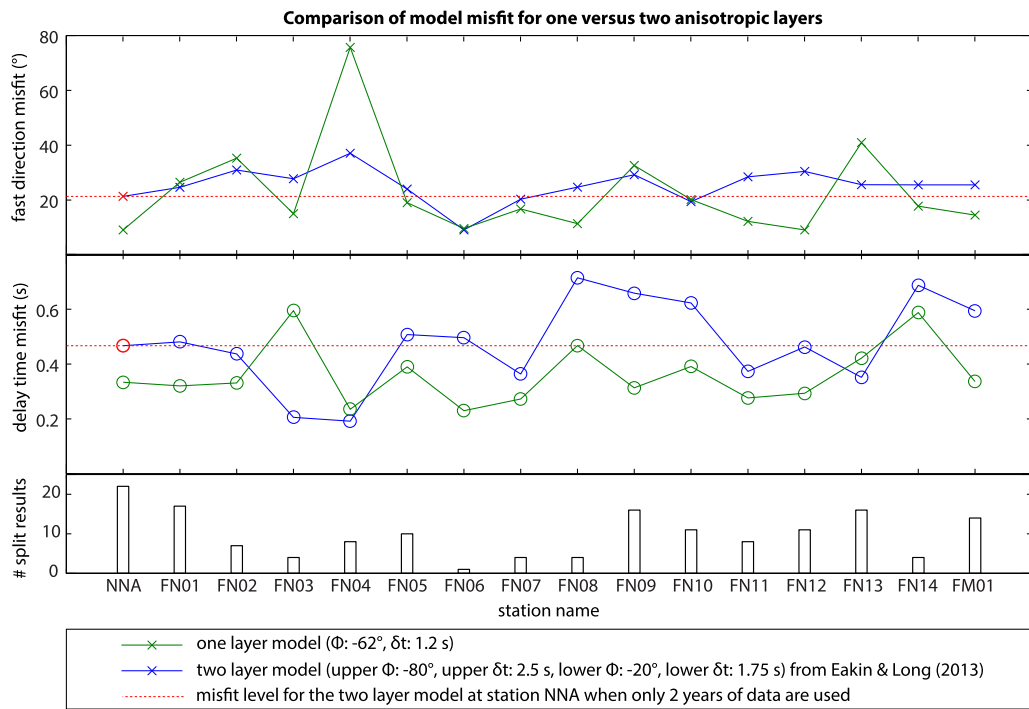


Fig. 5. Model predictions for the shear wave splitting pattern at seismic stations north of the Nazca Ridge with one versus two layers of anisotropy. Model misfit is calculated by finding the L_1 norm (sum of the absolute difference between the model predictions and splitting measurements). Total misfit at each station is divided by the number of results (bottom panel), to allow for comparability across the network. The values plotted in the top and middle panels therefore reflect the average misfit of the results from the model at each station. The one layer model is derived from the mean splitting parameters across the stations shown. The two-layer case is the best-fit model found by Eakin and Long (2013) using over 20 yr of data recording at station NNA and plotted in the upper left corner of Fig. 2a. When only two years of data are available (i.e. over the PULSE deployment), the fit of this two layer model across all the northern stations is comparable to that resolved at NNA with the same two years of data (red dotted line). (For interpretation of the references to color in this figure legend, the reader is referred to the web version of this article.)

The first three scenarios can be ruled out as explanations for our observations. For example, the first mechanism, in which the backazimuth is aligned in the fast or slow direction, would require that null measurements occur only at those specific backazimuths. The backazimuth distribution is limited for southern PULSE stations, but nulls are consistently recorded across the modest backazimuth range we do have, including events arriving from two or

three different backazimuth quadrants (Fig. S5). For the second or third mechanism (vertical mantle flow or upper mantle isotropy), we would expect source-side splitting measurements (which isolate sub-slab anisotropy) to also return nulls, especially given that the source-side measurements are made at the same frequency as SKS and therefore sample similar volumes of the upper mantle as SKS (i.e., their Fresnel zones are similar). However, source-

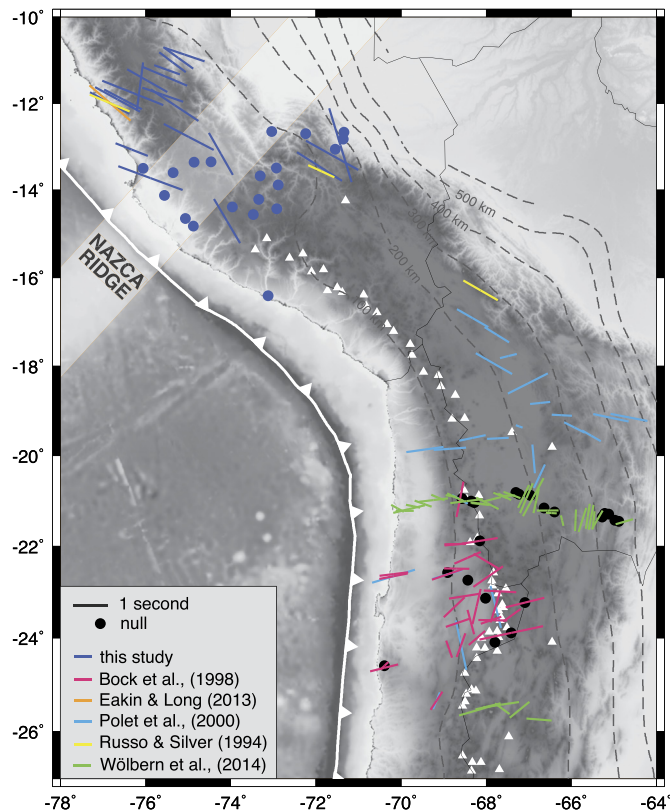


Fig. 6. Regional compilation of *KS splitting results both from previous studies and this study. For clarity purposes only the average (mean) result at each station has been plotted, to illustrate the spatial behavior of splitting dominated stations (colored bars), versus null dominated stations (large black dots). It is important to be aware that these station-averaged results hide the presence of any backazimuth variability and likely are a simplification of complex anisotropy at depth. For the results of this study, stations with more than 3 null measurements (and ≤ 3 split measurements) are designated as null stations. For PULSE or PeruSE stations with few measurements (i.e. ≤ 3 of either splits or nulls) are not plotted. Slab contours and volcano locations (white triangles) are the same as for Fig. 1.

side splitting measurements made on S phases originating from slab earthquakes near the southern part of our study area indicate 1–2 s of splitting with trench-oblique to sub-parallel fast directions (Eakin and Long, 2013) (Fig. 2a and Figs. 7–8). This suggests that the sub-slab mantle beneath the null region is substantially anisotropic, and that vertically propagating shear waves, such as

SKS, should accumulate splitting after traversing the sub-slab mantle.

Based on these source-side results, the anisotropic signal from the sub-slab mantle must therefore experience destructive interference somewhere in the upper layers of the subduction system when traversed by *KS (Fig. 8). The fourth mechanism mentioned above is a possibility. In this case, analytical equations for multiple layers of anisotropy suggest that from a theoretical point of view, two anisotropic layers cancel each other out (to produce apparent null splitting) when the fast directions of each layer differ by exactly 90° (Silver and Savage, 1994). The fast orientations must be exactly orthogonal to cancel, however, as a deviation as small as $\sim 5^\circ$ from orthogonality will still produce strong apparent splitting and non-nulls (e.g., Eakin and Long, 2013). The presence of widespread destructive interference from perfectly orthogonal layers throughout the wide region in which we observe dominantly null *KS splitting seems improbable, particularly since local S measurements (which sample supra-slab anisotropy) in south Peru display scattered or variable fast directions rather than a uniform geometry associated with a uniform upper layer (see Fig. 2 of Eakin et al., 2014).

We are left therefore with the fifth and final scenario, in which the upper mantle is anisotropic but that the anisotropy is strongly heterogeneous, with properties that vary rapidly laterally, or with depth, or both. Strong vertical heterogeneity in φ (where φ rotates as a function of depth, but the strength of anisotropy remains constant) has been shown to produce a strong scattering effect (Saltzer et al., 2000). This scattering effect results in reduced energy on the transverse component and smaller apparent delay times; if the scattering is strong, it can result in effectively null splitting. Similarly, Rümpker and Silver (1998) showed that for multiple layers of anisotropy with randomly assigned φ and δt within each layer the apparent δt accumulated through all the layers decreased as the number of layers increased. It is therefore possible for small delay times and null *KS arrivals to result from heterogeneity in φ , even when the strength of anisotropy may be constant. This could well be the case beneath the southern PULSE stations if there are many different layers of anisotropy at depth. In this scenario, however, it may be difficult to explain why we previously observed splitting of direct S phases with raypaths above and below the slab in the same region (Fig. 7), unless *KS phases traverse a strong heterogeneity in a region previously unsampled (i.e. within the slab).

If we consider the possibility of lateral heterogeneity, instead of variability with depth, we can imagine a similar scenario in

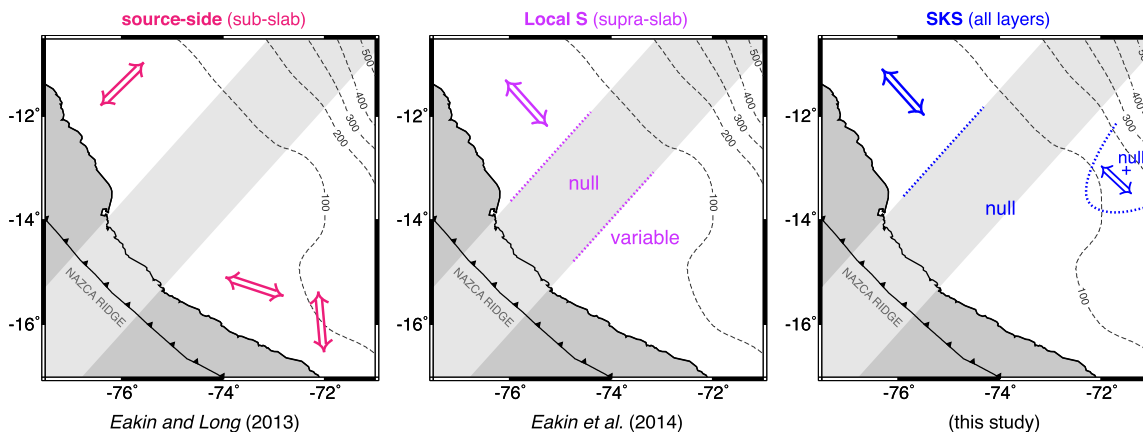


Fig. 7. Schematic overview of the regional splitting patterns found from studies of different shear-wave phases (local S , source-side teleseismic S , and *KS) across our study area. The predominant anisotropic fast directions within each region are plotted with schematic large arrows (not scaled by delay time). For the range of individual measurements see the papers listed at the bottom of each map. Slab contours are the same as for Fig. 1. All three maps show a change in anisotropic character from NW to SE across the Nazca Ridge.

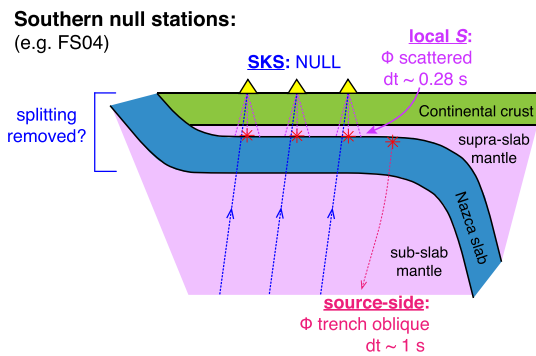


Fig. 8. Schematic diagram illustrating our preferred interpretation of *KS splitting measurements in the southern portion of our study region. The cartoon represents a 2D slice at the southern end of the Peruvian flat-slab region illustrating ray geometries for different shear wave phases and their corresponding shear wave splitting results. Source-side splitting measurements (pink) indicate that the sub-slab mantle is anisotropic, and local *S* measurements (purple) also indicate that the supra-slab is anisotropic. When SKS phases (blue) traverse the entire upper mantle, however the results are mostly null, suggesting that the SKS waves have not been split, or have undergone destructive interference along their raypath. (For interpretation of the references to color in this figure legend, the reader is referred to the web version of this article.)

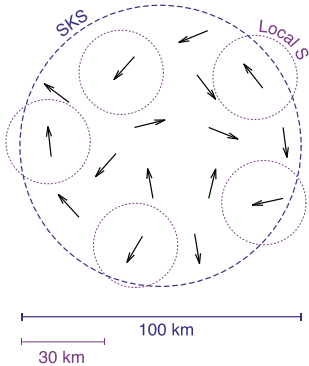


Fig. 9. An illustration (looking from above) of a possible mechanism for generating nulls at the southern stations with SKS phases. Small Fresnel zones of local *S* phases (purple circles) sample small pockets of uniform anisotropy. Larger Fresnel zones of SKS phases (blue circle) average over heterogeneous anisotropy resulting in no preferred orientation. Black arrows are representative of the fast direction (in the horizontal plane) at each location. (For interpretation of the references to color in this figure legend, the reader is referred to the web version of this article.)

which φ changes rapidly over relatively short distances, resulting in a similar scattering effect and generation of nulls. For this to occur φ must vary over distances smaller than the size of the first Fresnel zone (i.e. the volume over which seismic phases are most sensitive). There is already evidence for lateral anisotropic heterogeneity above the slab from our local *S* splitting dataset (Eakin et al., 2014), which found scattered and variable fast directions south of the Nazca Ridge (Fig. 7), but relatively constant δt . The local *S* phases, however have a relatively high frequency content, with an average characteristic frequency of ~ 1.2 Hz. The width of the first Fresnel zone at mantle depths is therefore small (~ 30 km; Gudmundsson, 1996). The *KS phases, in contrast, are much lower frequency (~ 0.08 Hz) and the Fresnel width is an order of magnitude larger (> 100 km). *KS phases would therefore average over the larger distances, obscuring the smaller scale heterogeneities reflected in the splitting of local *S* phases (Fig. 9). A plausible scenario, therefore, is that the splitting signal accrued from the sub-slab mantle undergoes destructive interference due to strong anisotropic heterogeneity in the shallow upper mantle.

It is unclear, however, what precise character the shallow anisotropic heterogeneity must take in order to entirely wipe out

the sub-slab splitting signal ($\sim 1\text{--}2$ s lag time). Further work that implements a regionally specific model incorporating finite frequency effects is needed; such a model would invoke a coherent, uniform anisotropic fabric in a lower layer and heterogeneous anisotropy with lateral (and/or depth) variations in φ in the shallower mantle. Such a study is beyond the scope of the present work. There is some evidence however, from a finite frequency point of view, that shear wave splitting of relatively low frequency phases such as SKS (≤ 0.1 Hz), are more sensitive to anisotropy in the shallower layers of the upper mantle (Saltzer et al., 2000).

Overall, there is no completely satisfactory explanation for the predominance of null *KS measurements across the southern PULSE stations, and their occurrence remains puzzling, although the observations are robust. We favor shallow, small-scale heterogeneity (as reflected in local *S* splitting patterns) as a mechanism for destructive interference with splitting due to deeper anisotropy, but this remains speculative at this stage. Further work constraining the southward extent of the null region and carrying out finite-frequency forward modeling for heterogeneous anisotropy will likely further elucidate the elusive origin of the nulls.

Finally, the third subset of stations, to the east of Cusco (Fig. 2), displays a mixture of split and null arrivals, even over similar backazimuths (Fig. S5). This region is also located near a transition in slab geometry; it is located just to the east of the flat-slab segment where the slab contours begin to get closer and the slab begins to bend and re-subduct. The most likely possibility is that *KS phases measured at these stations may reflect a different or additional source of anisotropy associated with the dipping slab to the east. Source-side measurements with ray paths through the dipping portion of the slab indicate the presence of distinct intra-slab anisotropy (Eakin and Long, 2013).

6. Conclusion

Measurements of *KS splitting at PULSE (and other) stations reveal considerable lateral variations in anisotropic structure beneath the Peruvian flat slab region. Deformation in the mantle both below and above the slab likely represents the primary contribution to the splitting signal, but an additional source from anisotropy within the slab itself is plausible. We have documented three distinct characteristic patterns of *KS splitting in our study area: predominantly trench-parallel fast splitting directions along the PULSE northern line, predominantly null *KS arrivals in the southern part of our study area, and complex and variable splitting at stations to the north and east of Cusco. Our most important finding is the delineation of a sharp boundary in upper mantle seismic anisotropy (reflected in both local *S* and *KS splitting behavior) associated with the Nazca Ridge. This marked change in seismic anisotropy at the ridge implies that the ridge strongly influences how the surrounding mantle deforms. From this we infer that the Nazca Ridge is not merely a passive feature; rather, it alters the dynamics of the Peruvian flat slab system, at least in terms of deformation of the surrounding mantle. A complete understanding of its role in flat slab evolution, and whether this role is causative, will require additional constraints on the geometry, structure, composition, buoyancy, and state of stress of the subducting Nazca Ridge, along with more detailed imaging of the slab morphology. Analysis of the PULSE dataset is ongoing and includes body and surface wave tomography, receiver function analysis, earthquake location and moment tensor analysis. These will likely further our understanding and enable additional quantitative comparisons between shear wave splitting measurements and other indicators of slab structure at depth.

Acknowledgements

Collection of the PULSE dataset was facilitated by the PASSCAL program of the Incorporated Research Institutions for Seismology (IRIS), and we are grateful to PASSCAL personnel for their contributions. We thank all project participants from Yale University, University of Arizona, University of North Carolina at Chapel Hill, and the Instituto Geofísico del Perú who assisted with field-work. We are particularly grateful to Astrid Martinez Kowler and Cristóbal Condori for invaluable assistance with PULSE field logistics. The GSN and PULSE data used in this study were accessed via the IRIS Data Management System (DMS). We thank Rob Clayton and Paul Davis for facilitating access to data from eight stations of the PeruSE network. The PULSE experiment was supported by the National Science Foundation via grants EAR-0943962 (MDL), EAR-0944184 (LSW), and EAR-0943991 (SLB). Constructive comments from two anonymous reviewers helped to improve the paper.

Appendix A. Supplementary material

Supplementary material related to this article can be found online at <http://dx.doi.org/10.1016/j.epsl.2014.12.015>.

References

- Assumpção, M., Feng, M., Tassara, A., Julià, J., 2013. Models of crustal thickness for South America from seismic refraction, receiver functions and surface wave tomography. *Tectonophysics* 609, 82–96. <http://dx.doi.org/10.1016/j.tecto.2012.11.014>.
- Bazargani, M., Isacks, B.L., 1976. Spatial distribution of earthquakes and subduction of the Nazca plate beneath South America. *Geology* 4, 686–692. [http://dx.doi.org/10.1130/0091-7613\(1976\)4](http://dx.doi.org/10.1130/0091-7613(1976)4).
- Benoit, M.H., Long, M.D., King, S.D., 2013. Anomalously thin transition zone and apparently isotropic upper mantle beneath Bermuda: evidence for upwelling. *Geochem. Geophys. Geosyst.* 14, 4282–4291. <http://dx.doi.org/10.1002/ggge.20277>.
- Biryol, C.B., Beck, S.L., Zandt, G., Wagner, L.S., 2013. Slab Geometry Control on Mantle Flow Regime: a case study from Central South America Subduction Zone. In: AGU Fall Meeting 2013. San Francisco, CA.
- Bishop, B., Beck, S., Zandt, G., Kumar, A., Wagner, L., Long, M., Tavera, H., 2013. Receiver function study of the Peruvian Flat-Slab Region: initial results from PULSE. In: AGU Fall Meeting 2013. San Francisco.
- Bock, G., Kind, R., Rudloff, A., Asch, G., 1998. Shear wave anisotropy in the upper mantle beneath the Nazca Plate in northern Chile. *J. Geophys. Res.* 103 (B10), 24333–24345. <http://dx.doi.org/10.1029/98JB01465>.
- Bowman, J.R., Ando, M., 1987. Shear-wave splitting in the upper-mantle wedge above the Tonga subduction zone. *Geophys. J. Int.* 88, 25–41. <http://dx.doi.org/10.1111/j.1365-246X.1987.tb01367.x>.
- Cahill, T., Isacks, B.L., 1992. Seismicity and shape of the subducted Nazca Plate. *J. Geophys. Res.* 97, 17503. <http://dx.doi.org/10.1029/92JB00493>.
- Conrad, C.P., Behn, M.D., Silver, P.G., 2007. Global mantle flow and the development of seismic anisotropy: differences between the oceanic and continental upper mantle. *J. Geophys. Res.* 112. <http://dx.doi.org/10.1029/2006JB004608>.
- Couch, R., Whitsett, R.M., 1981. Structures of the Nazca Ridge and the continental shelf and slope of southern Peru. *Geol. Soc. Am. Mem.* 154, 569–586. <http://dx.doi.org/10.1130/MEM154>.
- Eakin, C.M., Long, M.D., 2013. Complex anisotropy beneath the Peruvian flat slab from frequency-dependent, multiple-phase shear wave splitting analysis. *J. Geophys. Res., Solid Earth* 118, 4794–4813. <http://dx.doi.org/10.1002/jgrb.50349>.
- Eakin, C., Obrebski, M., Allen, R., Boyarko, D., Brudzinski, M., Porritt, R., 2010. Seismic anisotropy beneath Cascadia and the Mendocino triple junction: interaction of the subducting slab with mantle flow. *Earth Planet. Sci. Lett.* 297, 627–632. <http://dx.doi.org/10.1016/j.epsl.2010.07.015>.
- Eakin, C.M., Long, M.D., Beck, S.L., Wagner, L.S., Tavera, H., Condori, C., 2014. Response of the mantle to flat slab evolution: insights from local S splitting beneath Peru. *Geophys. Res. Lett.* 41, 3438–3446. <http://dx.doi.org/10.1002/2014GL059943>.
- Espurt, N., Baby, P., Brusset, S., Roddaz, M., Hermoza, W., Regard, V., Antoine, P.-O., Salas-Gismondi, R., Bolaños, R., 2007. How does the Nazca Ridge subduction influence the modern Amazonian foreland basin? *Geology* 35, 515. <http://dx.doi.org/10.1130/G23237A1>.
- Feng, M., van der Lee, S., Assumpção, M., 2007. Upper mantle structure of South America from joint inversion of waveforms and fundamental mode group velocities of Rayleigh waves. *J. Geophys. Res.* 112. <http://dx.doi.org/10.1029/2006JB004449>.
- Gripp, A.E., Gordon, R.G., 2002. Young tracks of hotspots and current plate velocities. *Geophys. J. Int.* 150, 321–361. <http://dx.doi.org/10.1046/j.1365-246X.2002.01627.x>.
- Gudmundsson, O., 1996. On the effect of diffraction on traveltimes measurements. *Geophys. J. Int.* 124 (1), 304–314. <http://dx.doi.org/10.1111/j.1365-246X.1996.tb06372.x>.
- Gutscher, M.-A., 2002. Andean subduction styles and their effect on thermal structure and interplate coupling. *J. South Am. Earth Sci.* 15, 3–10. [http://dx.doi.org/10.1016/S0895-9811\(02\)00002-0](http://dx.doi.org/10.1016/S0895-9811(02)00002-0).
- Gutscher, M.-A., Olivet, J.-L., Aslanian, D., Eissen, J.-P., Maury, R., 1999. The “lost Inca Plateau”: cause of flat subduction beneath Peru? *Earth Planet. Sci. Lett.* 171, 335–341. [http://dx.doi.org/10.1016/S0012-821X\(99\)00153-3](http://dx.doi.org/10.1016/S0012-821X(99)00153-3).
- Gutscher, M., Spakman, W., Bijwaard, H., Engdahl, E., 2000. Geodynamics of flat subduction: seismicity and tomographic constraints from the Andean margin. *Tectonics* 19, 814–833.
- Hampel, A., 2002. The migration history of the Nazca Ridge along the Peruvian active margin: a re-evaluation. *Earth Planet. Sci. Lett.* 203, 665–679.
- Hampel, A., Kukowski, N., Bialas, J., Huebscher, C., Heinbockel, R., 2004. Ridge subduction at an erosive margin: the collision zone of the Nazca Ridge in southern Peru. *J. Geophys. Res., Solid Earth* 109. <http://dx.doi.org/10.1029/2003JB002593>.
- Hayes, G.P., Wald, D.J., Johnson, R.L., 2012. Slab1.0: a three-dimensional model of global subduction zone geometries. *J. Geophys. Res.* 117. <http://dx.doi.org/10.1029/2011JB008524>.
- Helffrich, G., Silver, P., Given, H., 1994. Shear-wave splitting variation over short spatial scales on continents. *Geophys. J. Int.* 119, 561–573. <http://dx.doi.org/10.1111/j.1365-246X.1994.tb00142.x>.
- Jung, H., Karato, S., 2001. Water-induced fabric transitions in olivine. *Science* 293, 1460–1463. <http://dx.doi.org/10.1126/science.1062235>.
- Jung, H., Katayama, I., Jiang, Z., Hiraga, T., Karato, S., 2006. Effect of water and stress on the lattice-preferred orientation of olivine. *Tectonophysics* 421, 1–22. <http://dx.doi.org/10.1016/j.tecto.2006.02.011>.
- Kaneshima, S., Silver, P.G., 1995. Anisotropic loci in the mantle beneath central Peru. *Phys. Earth Planet. Inter.* 88, 257–272. [http://dx.doi.org/10.1016/0031-9201\(94\)02981-C](http://dx.doi.org/10.1016/0031-9201(94)02981-C).
- Karato, S., Jung, H., Katayama, I., Skemer, P., 2008. Geodynamic significance of seismic anisotropy of the upper mantle: new insights from laboratory studies. *Annu. Rev. Earth Planet. Sci.* 36, 59–95. <http://dx.doi.org/10.1146/annurev.earth.36.031207.124120>.
- Katayama, I., Jung, H., Karato, S., 2004. New type of olivine fabric from deformation experiments at modest water content and low stress. *Geology* 32, 1045. <http://dx.doi.org/10.1130/G20805.1>.
- Kneller, E.A., van Keken, P.E., Karato, S., Park, J., 2005. B-type olivine fabric in the mantle wedge: insights from high-resolution non-Newtonian subduction zone models. *Earth Planet. Sci. Lett.* 237, 781–797. <http://dx.doi.org/10.1016/j.epsl.2005.06.049>.
- Kneller, E.A., van Keken, P.E., Katayama, I., Karato, S., 2007. Stress, strain, and B-type olivine fabric in the fore-arc mantle: sensitivity tests using high-resolution steady-state subduction zone models. *J. Geophys. Res.* 112, B04406. <http://dx.doi.org/10.1029/2006JB004544>.
- Lloyd, S., van der Lee, S., França, G.S., Assumpção, M., Feng, M., 2010. Moho map of South America from receiver functions and surface waves. *J. Geophys. Res.* 115. <http://dx.doi.org/10.1029/2009JB006829>.
- Long, M.D., Becker, T.W., 2010. Mantle dynamics and seismic anisotropy. *Earth Planet. Sci. Lett.* 297, 341–354. <http://dx.doi.org/10.1016/j.epsl.2010.06.036>.
- Long, M., Silver, P., 2008. The subduction zone flow field from seismic anisotropy: a global view. *Science* 319, 315–318.
- Long, M.D., Silver, P.G., 2009. Mantle flow in subduction systems: the sub-slab flow field and implications for mantle dynamics. *J. Geophys. Res.* 114. <http://dx.doi.org/10.1029/2008JB006200>.
- Ma, Y., Clayton, R., 2014. The crust and uppermost mantle structure of Southern Peru from ambient noise and earthquake surface wave analysis. *Earth Planet. Sci. Lett.* 395, 61–70.
- Phillips, K., Clayton, R.W., 2014. Structure of the subduction transition region from seismic array data in southern Peru. *Geophys. J. Int.* 196, 1889–1905. <http://dx.doi.org/10.1093/gji/gjt504>.
- Pilger, R., 1981. Plate reconstructions, aseismic ridges, and low-angle subduction beneath the Andes. *Geol. Soc. Am. Bull.* 92, 448–456.
- Pilger, R.H., Handschuhmacher, D.W., 1981. The fixed-hotspot hypothesis and origin of the Easter-Sala y Gomez-Nazca trace. *Geol. Soc. Am. Bull.* 92, 437–446. [http://dx.doi.org/10.1130/0016-7606\(1981\)92<437:THFHH>2.0.CO;2](http://dx.doi.org/10.1130/0016-7606(1981)92<437:THFHH>2.0.CO;2).
- Pollet, J., Silver, P., Beck, S., Wallace, T., 2000. Shear wave anisotropy beneath the Andes from the BANJO, SEDA, and PISCO experiments. *J. Geophys. Res.* 105, 6287–6304.
- Rosenbaum, G., Giles, D., Saxon, M., Betts, P.G., Weinberg, R.F., Duboz, C., 2005. Subduction of the Nazca Ridge and the Inca Plateau: insights into the formation of ore deposits in Peru. *Earth Planet. Sci. Lett.* 239, 18–32. <http://dx.doi.org/10.1016/j.epsl.2005.08.003>.
- Rümpker, G., Silver, P., 1998. Apparent shear-wave splitting parameters in the presence of vertically varying anisotropy. *Geophys. J. Int.* 135, 790–800.

- Russo, R., Silver, P., 1994. Trench-parallel flow beneath the Nazca Plate from seismic anisotropy. *Science* 263, 1105–1111.
- Saltzer, R.L., Gaherty, J.B., Jordan, T.H., 2000. How are vertical shear wave splitting measurements affected by variations in the orientation of azimuthal anisotropy with depth? *Geophys. J. Int.* 141 (2), 374–390. <http://dx.doi.org/10.1046/j.1365-246x.2000.00088.x>.
- Siebert, L., Simkin, T., 2002. Volcanoes of the World: an illustrated catalog of Holocene volcanoes and their eruptions. Smithsonian Institution, Global Volcanism Program Digital Information Series. GVP-3. <http://www.volcano.si.edu/world/>.
- Silver, P., Chan, W., 1991. Shear wave splitting and sub continental mantle deformation. *J. Geophys. Res., Solid Earth* 96, 16429–16454.
- Silver, P.G., Savage, M.K., 1994. The interpretation of shear-wave splitting parameters in the presence of two anisotropic layers. *Geophys. J. Int.* 119, 949–963. <http://dx.doi.org/10.1111/j.1365-246X.1994.tb04027.x>.
- Skinner, S.M., Clayton, R.W., 2011. An evaluation of proposed mechanisms of slab flattening in Central Mexico. *Pure Appl. Geophys.* 168, 1461–1474. <http://dx.doi.org/10.1007/s00024-010-0200-3>.
- Skinner, S.M., Clayton, R.W., 2013. The lack of correlation between flat slabs and bathymetric impactors in South America. *Earth Planet. Sci. Lett.* 371–372, 1–5. <http://dx.doi.org/10.1016/j.epsl.2013.04.013>.
- Van der Meijde, M., Julià, J., Assumpção, M., 2013. Gravity derived Moho for South America. *Tectonophysics* 609, 456–467. <http://dx.doi.org/10.1016/j.tecto.2013.03.023>.
- Walpole, J., Wookey, J., Masters, G., Kendall, J.M., 2014. A uniformly processed data set of SKS shear wave splitting measurements: a global investigation of upper mantle anisotropy beneath seismic stations. *Geochem. Geophys. Geosyst.* 15, 1991–2010. <http://dx.doi.org/10.1029/2014GC005278>.
- West, J.D., Fouch, M.J., Roth, J.B., Elkins-Tanton, L.T., 2009. Vertical mantle flow associated with a lithospheric drip beneath the Great Basin. *Nat. Geosci.* 2, 439–444. <http://dx.doi.org/10.1038/ngeo526>.
- Wölbern, I., Löbl, U., Rümpker, G., 2014. Crustal origin of trench-parallel shear-wave fast polarizations in the Central Andes. *Earth Planet. Sci. Lett.* 392, 230–238. <http://dx.doi.org/10.1016/j.epsl.2014.02.032>.
- Woods, M.T., Okal, E.A., 1994. The structure of the Nazca ridge and Sala y Gomez seamount chain from the dispersion of Rayleigh waves. *Geophys. J. Int.* 117, 205–222. <http://dx.doi.org/10.1111/j.1365-246X.1994.tb03313.x>.
- Wüstefeld, A., Bokelmann, G., 2007. Null detection in shear-wave splitting measurements. *Bull. Seismol. Soc. Am.* 97, 1204–1211. <http://dx.doi.org/10.1785/0120060190>.
- Wüstefeld, A., Bokelmann, G., Zaroli, C., Barruol, G., 2008. SplitLab: a shear-wave splitting environment in Matlab. *Comput. Geosci.* 34, 515–528. <http://dx.doi.org/10.1016/j.cageo.2007.08.002>.